JGR Atmospheres

RESEARCH ARTICLE
10.1029/2019JD030286

Investigating an Unusually Large 28-Day Oscillation in Mesospheric Temperature Over Antarctica Using Ground-Based and Satellite Measurements

Yucheng Zhao[1], M. J. Taylor[1], P.-D. Pautet[1], T. Moffat-Griffin[2], M. E. Hervig[3], D. J. Murphy[4], W. J. R. French[4], H. L. Liu[5], W. R. Pendleton Jr[1], and J. M. Russell III[6]

[1]Center for Atmospheric and Space Sciences, Utah State University, Logan, UT, USA, [2]British Antarctic Survey, Cambridge, UK, [3]GATS, Inc., Newport News, VA, USA, [4]Australian Antarctic Division, Hobart, Tasmania, Australia, [5]HAO, NCAR, Boulder, CO, USA, [6]Center for Atmospheric Sciences, Hampton University, Hampton, VA, USA

Key Points:
- A large amplitude, persistent 28-day mesospheric temperature planetary wave event was detected over Antarctica as part of the ANGWIN measurement network
- A novel combination of ground-based Antarctic measurements and satellite temperature data was utilized
- The 28-day periodicity and the global signatures of this oscillation are similar to the predicted Rossby (1,4) mode

Correspondence to:
Y. Zhao,
yu.cheng@usu.edu

Citation:
Zhao, Y., Taylor, M. J., Pautet, P.-D., Moffat-Griffin, T., Hervig, M. E., Murphy, D. J., et al. (2019). Investigating an unusually large 28-day oscillation in mesospheric temperature over Antarctica using ground-based and satellite measurements. *Journal of Geophysical Research: Atmospheres*, *124*. https://doi.org/10.1029/2019JD030286

Received 9 JAN 2019
Accepted 12 JUL 2019
Accepted article online 24 JUL 2019

Abstract The Utah State University Advanced Mesospheric Temperature Mapper was deployed at the Amundsen-Scott South Pole Station in 2010 to measure OH temperature at ~87 km as part of an international network to study the mesospheric dynamics over Antarctica. During the austral winter of 2014, an unusually large amplitude ~28-day oscillation in mesospheric temperature was observed for ~100 days from the South Pole Station. This study investigates the characteristics and global structure of this exceptional planetary-scale wave event utilizing ground-based mesospheric OH temperature measurements from two Antarctic stations (South Pole and Rothera) together with satellite temperature measurements from the Microwave Limb Sounder on the Aura satellite and the Solar Occultation For Ice Experiment on the Aeronomy of Ice in the Mesosphere satellite. Our analyses have revealed that this large oscillation is a wintertime, high-latitude phenomenon, exhibiting a coherent zonal wave #1 structure below 80-km altitude. At higher altitudes, the wave was confined in longitude between 180°E and 360°E. The amplitude of this oscillation reached ~15 K at 85 km, and it was observed to grow with altitude as it extended from the stratosphere into the lower thermosphere in the Southern Hemisphere. The satellite data further established the existence of this oscillation in the Northern Hemisphere during the boreal wintertime. The main characteristics and global structure of this event as observed in temperature are consistent with the predicted 28-day Rossby Wave (1,4) mode.

1. Introduction

Planetary waves (PWs) are global-scale phenomena generated in the lower atmosphere which can propagate upward into the upper Mesosphere and Lower Thermosphere (MLT) region under the right conditions, interacting with gravity waves and tides and playing an important role in MLT dynamics. Due to their relatively low phase speeds, PWs are prone to filtering by the background wind field before reaching the MLT region. Nonetheless, mesospheric PWs have been observed utilizing satellite and ground-based measurements at all latitudes in mesospheric wind and temperature data (e.g., Lieberman & Riggin, 1997; Luo et al., 2001; Murphy et al., 2007; Riggin et al., 1995; Sivjee et al., 1994; Walterscheid et al., 2015; Wu et al., 1994).

To date, ground-based mesospheric PW observations over Antarctica are sparse. Table 1 summarizes reports of Antarctica mesospheric PW observations since the 1980s. Most measurements have been made using partial reflection (60–105 km) and meteor radar (80–100 km) techniques and more recently using temperature measurements from OH spectrometer. Some studies involved multistations (e.g., Espy et al., 2005), and others used multiyear data (e.g., Stockwell et al., 2007). These studies have succeeded in identifying PWs with periods of 2, 4, 5, 14, 16, and 30–50 days with the later using 9 years of data.

South Pole (SP) station (90°S) is a unique location on Earth for mesospheric dynamic measurements. Optical observations can be made continuously over a 4 –5 month period during the extended winter season. Starting in the early 1990s, two long-term data sets were obtained, both utilizing the OH emission at ~87-km altitude to observe the mesospheric temperature, wind, and OH intensity using a Fabry-Perot spectrometer (e.g., Hernandez, 2003) and OH temperature and brightness using a Michelson Interferometer (e.g., Azeem et al., 2007; Sivjee & Walterscheid, 1994). In 1995, a meteor radar system was deployed at SP station and mesospheric wind measurements (80–100 km) were conducted with more than 1 year of operations providing

Table 1
Summary of Mesospheric PW Measurements Over Antarctica

Period	Location	References	Data type
2 days	Rothera (UK)	Tunbridge and Mitchell (2009)	Radar wind
4 days	Scott base (NZ) and Mauson base (NZ)	Lawrence et al. (1995)	Radar wind
5 days	Rothera (UK; 4 years)	Day and Mitchell (2010)	Radar wind
14 days	Rothera (UK), Halley (UK), Sanae (SA), Syowa (JP), and Davis (AU; 9 years)	French et al. (2005), Dowdy et al. (2004), Espy et al. (2005), and Stockwell et al. (2007)	Radar wind and OH temperature
16 days	Rothera (UK) and Troll (NO) stations	Demissie et al. (2013)	OH temperature, O_3 volume, and mixing ratio (34–80 km)
30–50 days	Davis (AU), Rothera (UK), Halley (UK), Sanae (SA), and Syowa (JP)	Espy et al. (2005) and Stockwell et al. (2007)	Radar wind and OH temperature

Note. PW = Planetary wave.

continuous day-night (summer/winter) measurements (e.g., Forbes et al., 1999; Palo et al., 1998). Subsequently, Fe/Rayleigh lidar observations of iron density and mesospheric temperature profiles were obtained during 1999–2001, extending from 30 to 110 km depending on the Fe density (e.g., Chu et al., 2002). These data sets have provided valuable insights into mesospheric temperature/wind structures and climatology as well as tides and PWs, primarily during the wintertime (e.g., Azeem et al., 2007; Azeem & Sivjee, 2009; Forbes et al., 1999; Hernandez, 2003; Hernandez et al., 1992; Pan & Gardner, 2003; Sivjee & Walterscheid, 2002).

This said, very few mesospheric PW events from SP have been reported. Fraser et al. (1993) investigated an eastward moving mesospheric 2–4 day wave using Fabry-Perot spectrometer wind measurements, revealing zonal wave #1 structure. Using mesospheric wind data obtained by the same instrument, Hernandez et al. (1997) analyzed an ~2 day (51.8 hr) standing wave event. Sivjee and Walterscheid (2002) identified low-frequency intraseasonal variations of 17, 23, and 45 days in the mesosphere, using three winter seasons of OH (3,1) band brightness data obtained with a Michelson Interferometer. Using meteor radar wind data, Palo et al. (1998) reported eastward propagating long-period wave activity and Forbes et al. (1999) confirmed that in addition to strong tidal oscillations, eastward propagating PWs existed during the winter seasons with period of 2–10 days. However, to our best knowledge, there have been no reports of PWs in mesospheric temperature over SP and no prior reports of 28-day oscillation over Antarctica.

As part of the Antarctic Gravity Wave Instrument Network (ANGWIN), the Utah State University (USU) Advanced Mesospheric Temperature Mapper (AMTM) was deployed at SP Station in 2010. Since then, high-quality continuous OH rotational temperature and band intensity measurements have been obtained from SP during the extended winter season (Pautet et al., 2018). In this paper, we utilize the ground-based OH temperature measurements from SP and from Rothera station, together with satellite temperature measurements to investigate the characteristics and global structures of an unusually large 28-day oscillation observed during the austral winter of 2014. In this paper, Section 2 will introduce the data used for this study. Section 3 will present the results from the ground-based temperature measurements and the temporal evolution of this event. Section 3 will also examine the characteristics and spatial structure of this large oscillation using available satellite temperature data (Solar Occultation For Ice Experiment [SOFIE]/Aeronomy of Ice in the Mesosphere [AIM] and Microwave Limb Sounder [MLS]/Aura). Section 4 will discuss the possible origin of this 28-day oscillation. A summary of the results is given in section 5.

2. Instrumentation and Data

2.1. SP Station

The USU AMTM is a novel instrument designed to map dynamical structures in mesospheric temperatures in the upper atmosphere using observations of the infrared OH (3,1) band emission at ~1.55 μm. This well-known airglow emission originates from an ~7 –8 km (full width at half maximum) layer located at a nominal altitude of ~87 km and has been widely used as a tracer of a broad range of dynamical processes including gravity waves, tides, PWs, and seasonal variations present in the mesopause region. (e.g., Baker & Stair, 1988; Cai et al., 2014; French & Klekociuk, 2011; Meriwether, 1975;

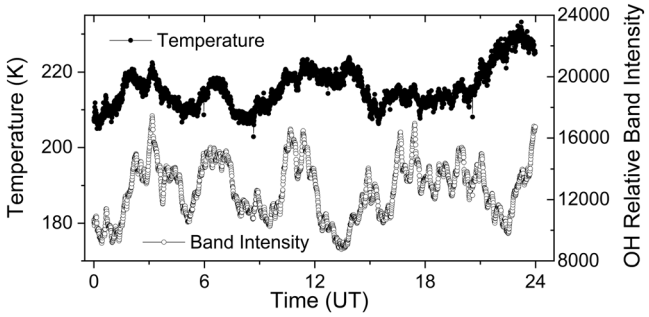

Figure 1. Daily OH temperature (solid circles) and OH relative band intensity (open circles) on 17 May (DOY 138), 2012 from South Pole station.

Pendleton et al., 2000; Sivjee & Walterscheid, 2002; Taylor et al., 2007; Zhao et al., 2007). The AMTM uses a wide field (120°) telecentric imaging system to sequentially observe the $P_1(2)$ and $P_1(4)$ emission lines of the OH (3,1) band and a selected background region to obtain high precision OH rotational temperature maps (typical zenith field of view ~200 × 160 km), using the well-established "ratio" method (e.g., Meriwether, 1975). In operation, time series of band intensity and temperature maps are obtained every ~30 s, with a zenith spatial resolution of ~0.6 km/pixel. Cross-calibration observations alongside a Na wind temperature lidar at USU indicate a typical precision of ~2 K/pixel and an accuracy of ~5 K with respect to coincident height-weighted (full width at half maximum ~8 km) lidar measurements using a mean altitude of 87 km (Pautet et al., 2014). The first AMTM developed at USU was deployed to the U.S. Amundsen-Scott SP Station in January 2010 and has operated successfully with continuous (24 hr) observations during each winter season (from late April to the end of August, ~4.5 months) from 2011 to date.

Figure 1 shows a typical example of AMTM continuous measurements of zenith OH temperature and band intensity during a 24-hr period on day of year (DOY) 138 (17 May) of 2012. The temperature (solid circles) and band intensity (open circles) are the mean of the 20 by 20 center pixels (referred as zenith temperature and intensity hereafter) of the AMTM data with a temporal resolution of ~30 s and a daily total of ~2500 temperature and band intensity measurements. The temperature and the band intensity both show gravity wave activity with periods ranging from ~1 hr to several hours. Further spectral analysis of the wintertime temperature measurements (not shown) indicates that the gravity wave activity usually dominated the wave spectrum during the winter season at the pole, while the tides are either not present in our data or very weak compared to the shorter period gravity waves. Figure 2 shows the winter season 2012 daily (24 hr) mean temperature and band intensity (17 April to 29 August, 2012). In 2012, our winter season measurements started at DOY 108 (April 17) when the temperature and band intensity were at their highest levels, and they both then decreased throughout the winter. The early season OH temperatures were high at ~220 K in April and proceeded to decrease throughout the season down to ~205 K with a winter mean of 212 K. Similar decline was detected in mean seasonal temperatures from ~207 K in April to ~200 K in August with a winter mean of 204 K from Davis station (68.6°S, 78.0°E; result not shown). One striking feature of the SP daily mean temperature and band intensity is the superimposed oscillations upon the observed linear seasonal decreasing trend. A Lomb-Scargle periodogram analysis (Press et al., 1992; Scargle, 1982) of the AMTM temperature data revealed a very rich PW spectrum (Figure 3), with periods of ~5, ~18, ~28, and ~45 days. As noted earlier, similar intraseasonal variations with periodicities of 17, 23, and 45 days were also reported from SP by Sivjee and Walterscheid (2002) but only in OH (3,1) band brightness. In this study, we will focus on the AMTM temperature data from SP station obtained during the winter season of 2014 when an unusually large amplitude 28-day oscillation was observed. The data are available online (http://digitalcommons.usu.edu/ail/. Password to access the database can be provided upon request to the authors).

2.2. Rothera Station

Rothera Research Station is a British Antarctic Survey base situated on Adelaide Island immediately to the west of the Antarctic Peninsula (67.6°S, 68.1°W). An OH Bomen spectrometer has been operated at Rothera since 2002, providing mesospheric temperature measurements as part of the ANGWIN program. The spectrometer observed the OH Meinel band nightglow emission over the 1,000–1,700 nm spectral range at ~0.5 nm resolution to measure the OH band radiance and to derive its rotational temperature. Interferograms were obtained every 3 s, and the data were integrated for periods between ~5 and 15 min for each spectrum, depending upon the radiance levels. The relative uncertainty estimates for integrated rotational temperature were typically 3–5%. Continuous nocturnal measurements were made for solar depression angle >5°. Further

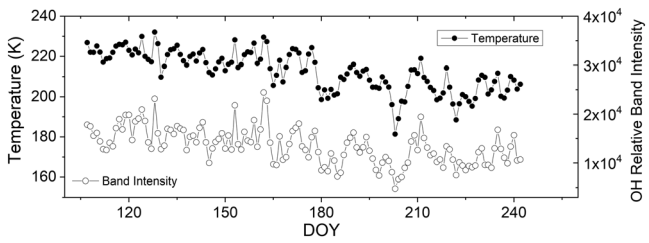

Figure 2. Daily mean zenith temperature (solid circles) and OH (3,1) relative band intensity (open circles) for the 2012 winter season at South Pole station.

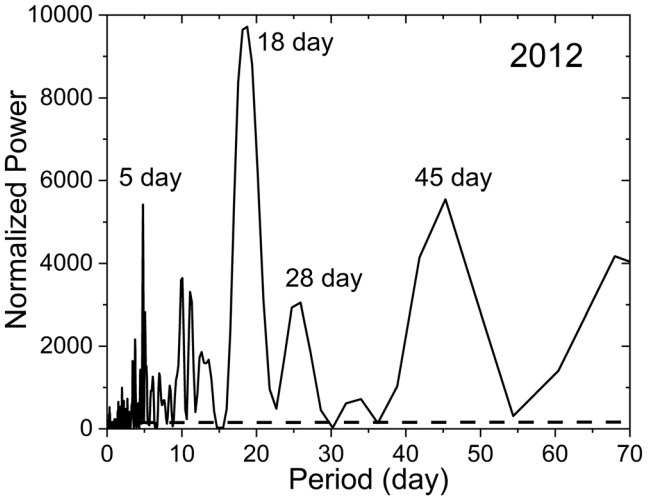

Figure 3. Lomb-Scargle periodogram results for winter 2012, revealing a rich spectrum of planetary waves. The dashed line shows the 95% confidence level.

details of the instrument operations and the spectral and wavelength calibrations are described by Espy and Stegman (2002) and Espy et al. (2003, 2007).

In this paper, we use the 2014 daily mean OH (3,1) temperature from Rothera. Observations started on 19 Feb (DOY 49) and continued until 22 Oct (DOY 294), yielding a total of 199 nights of data. For spectral analysis and band-pass filtering, the daily mean data were then resampled to 1-day intervals by applying a standard spline interpolation to eliminate data gaps (days of missing data due to weather condition). The Rothera temperature data are available online (http://psddb.nerc-bas.ac.uk/data/access/coverage.php?menu=4&bc=1&source=1&class=46&year=2014).

2.3. Satellite Measurements

The NASA AIM satellite was launched in April 2007 as the first satellite mission dedicated to investigating Polar Mesospheric Clouds (Russell et al., 2009). SOFIE is one of the two main instruments onboard the AIM satellite. SOFIE conducts solar occultation measurements to retrieve chemical composition of several key atmospheric species and Polar Mesospheric Clouds properties (Gordley et al., 2009). In particular, each day, a total of 15 high-latitude vertical temperature profiles are obtained at sunset (Southern Hemisphere) and 15 at sunrise (Northern Hemisphere). In this study, we utilize the 2014 SOFIE temperature measurements (version 1.3, level 2, Hervig & Gordley, 2010; and Hervig et al., 2016) from 15 to 100 km at 1-km intervals in both hemispheres. The precision of v1.3 SOFIE temperature is within 0.2 K with 2–4 K warm bias compared to SABER temperature during the summer at NLC altitudes (~83 km) and larger above 88 km (Gordley et al., 2009; Hervig et al., 2016 and Stevens et al., 2012). The SOFIE data are available as standard data products online (http://sofie.gats-inc.com/sofie/index.php). Within the year of 2014, the SOFIE measurements covered the latitude range 48°S to 72°S in the Southern Hemisphere and 61–89°N in the Northern Hemisphere.

The MLS on the NASA Aura satellite was launched on 15 July 2004 (Schoeberl et al., 2006; Waters et al., 2006). As a key data product, global temperature profiles are continuously obtained from ~9 to ~90 km with a total of 240 vertical scans each orbit, covering the latitude range 83°S to 83°N. The MLS temperature precision decreased with altitude, from 0.6 K in the stratosphere to 2.5 K in the mesosphere (e.g., Schwartz et al., 2008). In this study, we have used the high-latitude SOFIE temperature profiles together with the MLS v4.2 global temperature retrievals from 2014 (https://disc.gsfc.nasa.gov/datasets?page=1&keywords=ML2T_004) to investigate the global and vertical structures of the observed long period ~28-day mesospheric oscillation.

3. Observations and Results

3.1. Ground-Based Observations and Results

In 2014, the USU AMTM at SP began taking data in April (DOY 108) and the measurements stopped at the end of August (DOY 245) when the sky became too bright due to twilight. A total of 136 days of near 24-hr continuous measurements of the OH (3,1) band relative intensity and derived rotational temperature were obtained, with short data gaps occasionally, caused by clouds. Figure 4a shows the 24-hr daily mean AMTM zenith temperature (thin line with solid circles), while the dashed curve shows a second-order polynomial fit of the temperature data to illustrate the general temperature trend during this winter season. The fit shows that the MLT temperature initially increased during April and May, reaching an annual maximum around the end of May and decreased thereafter, until the end of the winter season, agreeing well with previous MLT temperature studies (e.g., Azeem et al., 2007; Hernandez, 2003). The mean of the winter season was 211.5 K with a large standard deviation of 13.3 K. Figure 4b shows the temperature perturbation with the trend (dashed line) removed. A large oscillation is evident, starting in the middle of the winter, around end of May (~DOY 150) and observed continuously for nearly 100 days until the end of the winter season (~DOY 245). To investigate the period of this strong oscillation, a Lomb-Scargle periodogram

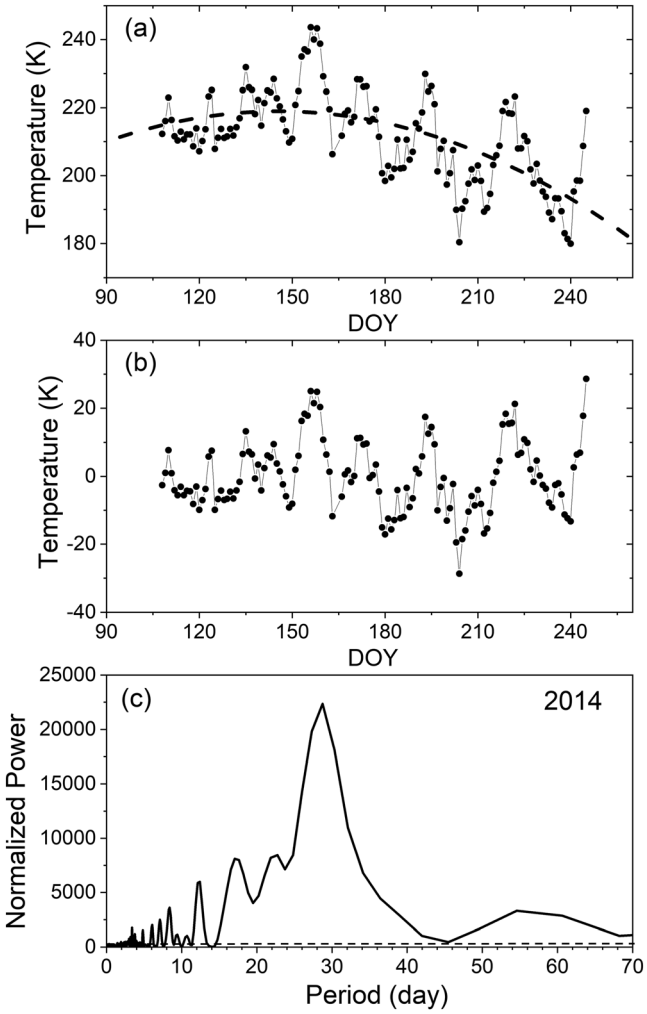

Figure 4. (a) Plot of daily mean temperature versus DOY dates for winter 2014. The dashed line depicts a second-order polynomial fit to the temperature data. (b) Same data with the fit removed, showing the large temperature oscillation, growing in amplitudes during the course of the winter. (c) Lomb-Scargle periodogram of these data revealing a remarkably prominent 28-day oscillation along with 5-, 8-, 12-, and 17-day oscillations. The dashed line shows the 95% confidence level. DOY = day of year.

analysis was applied to the full winter temperature data set, using the 30-s temporal resolution, resulting in a high confidence level in the analysis. The resultant power spectrum is plotted in Figure 4c and is dominated by a single peak with a well-defined period of ~28 days (see appendix for statistical confidence analysis of this event). This peak dwarfs the other PW signatures (i.e., 5, 8, 12, and 17 days) that were also detected by the AMTM with high confidence during this winter season.

As illustrated previously in Figure 3, PWs with similar 28-day periodicity in MLT temperature data have been detected by the AMTM at SP but have never reached such large amplitudes (13.5 K) as observed during the winter of 2014. To investigate this prominent oscillation further, we have examined data from two other Antarctic sites, Rothera (67.6°S, 68.1°W) and Davis (68.6°S, 78.0°E) stations, where coincident mesospheric temperature measurements were obtained as part of the ANGWIN program. Both Rothera and Davis are located at similar and significantly lower latitudes (>20° lower), and consequently, their winter season nighttime measurements at these sites started about 2 months earlier and ended about 2 months later than at SP, providing valuable additional observation time. The duration of their daily measurements ranged from ~4 hr (beginning and end of the winter season) to 24 hr around solstice. Figure 5 plots the Rothera 2014 daily mean OH (3,1) band temperature (black curve) together with the daily mean temperature (red curve) from

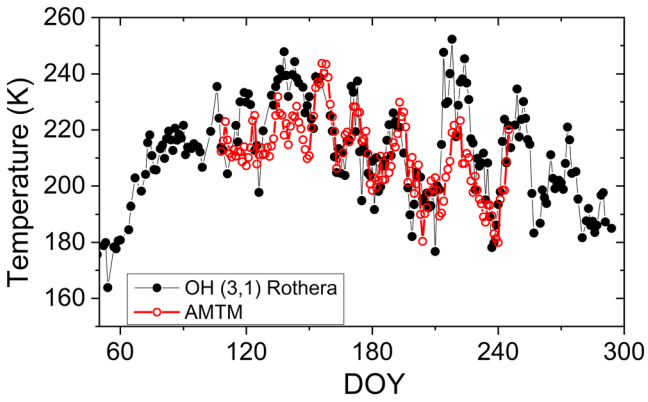

Figure 5. Comparison of 24-hr mean temperature from South Pole (red) and nightly mean temperature from Rothera (black). The coherent growth of the 28-day oscillation is evident in both data sets starting around day 180. Note the additional two cycles measured at Rothera due to extended observing period. DOY = day of year; AMTM = Advanced Mesospheric Temperature Mapper.

SP (as in Figure 4a). The extended winter seasonal mean at Rothera was 211.4 K, similar to that at SP, while the standard deviation at Rothera (17.6 K) was even larger than at SP. Furthermore, the extended Rothera data revealed two additional cycles of this 28-day oscillation. Close inspection of Figure 5 shows that the mesospheric temperatures from these two stations exhibited the same in-phase, large amplitude oscillations superimposed on a similar seasonal trend during the winter of 2014, providing exceptional confidence in the quality of these two data sets. This said, a similar analysis of the 2014 OH spectrometer temperature data from Davis station (longitude 78.0°E) indicated no significant evidence of this 28-day oscillation in the MLT region. This very surprising and important result is discussed further in section 3.2 and later.

To investigate the periodicity and duration of the waves seen in the Rothera data, a wavelet analysis (Torrence & Compo, 1998) was applied to the nightly mean OH temperature data and the results are shown in Figure 6. During the early winter season, waves with periods ~13–16 days were detected but only briefly. The dominant PW activity started in June (around DOY 180) and initially exhibited a broad range of periods between ~20 and 40 days, which subsequently evolved into the strong 28-day oscillation (peaking between DOY 220 and 230) and then remained prominent throughout the rest of the winter and into the early spring season, with final observations limited by twilight.

In order to more quantitatively compare these long period oscillations as detected from both sites, a band-pass filter (24–30 day) was applied to the nightly mean temperature data from Rothera and the corresponding 10-min resolution temperature data from SP. The results are shown in Figure 7 and are most revealing. At each site, the wave appeared at the same time (DOY 150) and the subsequent cycles of this 28-day oscillation exhibited high phase coherence during the rest of the winter season (>140 days). Furthermore, both 28-day oscillations were observed to grow uniformly in amplitude during the first two cycles, peaking around DOY 220 and then decaying together. The maximum amplitude at Rothera reached ~15.5 K and was ~15% larger than that at SP (13.5 K). The longer Rothera data set mapped five full cycles of this event at the MLT (~87 km) altitude.

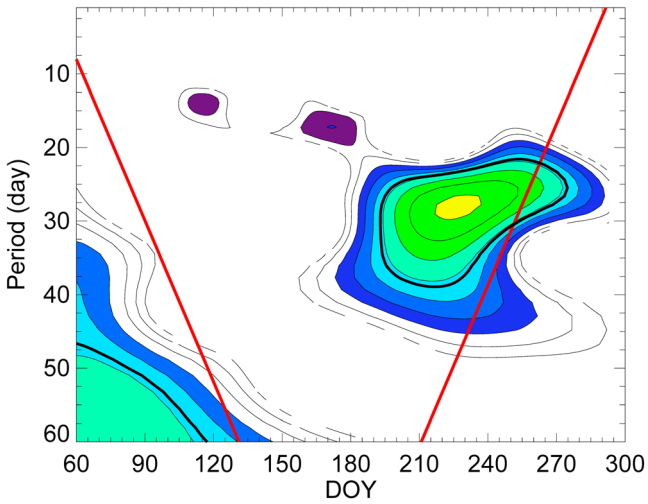

Figure 6. Wavelet analysis of the Rothera OH nightly mean temperatures winter season 2014 showing the evolution of the 28-day oscillation. The bold black lines define the 95% confidence level, and the red lines define the "cone of influence." Periods outside the cone of influence are subject to edge effect. DOY = day of year.

This is the first time that such a long duration, large amplitude, coherent 28-day oscillation has been reported in mesospheric temperature. Our SP and Rothera ground-based data sets have firmly established the existence, periods, and duration of this remarkable event as observed in the polar 2014 winter MLT region over Antarctica.

3.2. Satellite Observations and Results

We now explore the vertical and horizontal extent and duration of this prominent 28-day PW event utilizing available complementary temperature measurements obtained by the NASA AIM and Aura satellites.

The SOFIE temperature profiles (15–100 km) from the AIM satellite, with the highest quality vertical resolutions, were used first to investigate the time evolution of the vertical structure of this large oscillation. A Fast Fourier Transform (FFT) spectral analysis was first applied to the SOFIE temperature at 85 km between 270°E and 300°E. This location was chosen based on our ground-based results showing that larger amplitudes of this 28-day oscillation were observed over Rothera station as discussed in section 3.1. The resultant spectrum is plotted in Figure 8. The spectrum is similar to that in Figure 4c, exhibiting a strong peak at 26–28 days. This established that

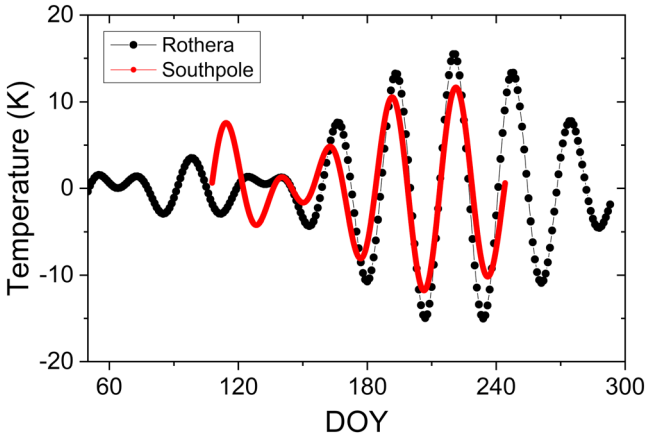

Figure 7. Band-pass filtered (24–30 days) temperatures from South Pole station (red) and Rothera station (black). Note the high coherence in the growth and the decay of the wave amplitudes at both sites. DOY = day of year.

both the satellite and ground-based temperature measurements detected this strong 28-day oscillation in the MLT region. To further examine the vertical extent of this event, the 2014 southern hemispheric SOFIE temperature between 270°E and 300°E were filtered using the same (24–30 days) band-pass filter as that applied to the ground-based data. Figure 9 plots the results as function of DOY versus altitude. The oscillation was first detected around DOY 150 around 60 km, commensurate with the ground-based measurements. The combined results show that the event extended vertically throughout the stratosphere into the upper MLT. The amplitude of this oscillation exhibited a broad maximum around 85 km (extending from ~80 to 90 km) that grew during the first three cycles and peaking around DOY 223. Thereafter, the PW amplitude decreased over the next three cycles and finally disappeared after DOY 300 (end of October), as observed in the ground-based measurements.

In order to investigate the temporal variation in the zonal structure of this event, the SOFIE 2014 temperature data were binned into 30° longitude sectors at all altitudes, and the same band-pass filter was then applied to each sector. The filtered results at 85 km (in close proximity to the nominal OH layer peak altitude) are plotted in Figure 10 and reveal a prominent geographically localized signature in the MLT region during

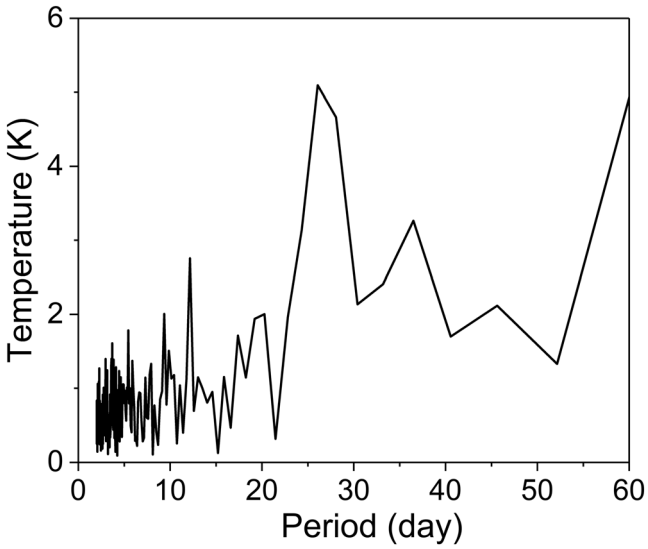

Figure 8. Spectrum analysis results using Southern Hemisphere Solar Occultation For Ice Experiment (SOFIE) temperature at 85 km between 270°E and 300°E longitudes for 2014. The result shows a distinct peak at 26–28 days, consistent with the results of ground-based analysis.

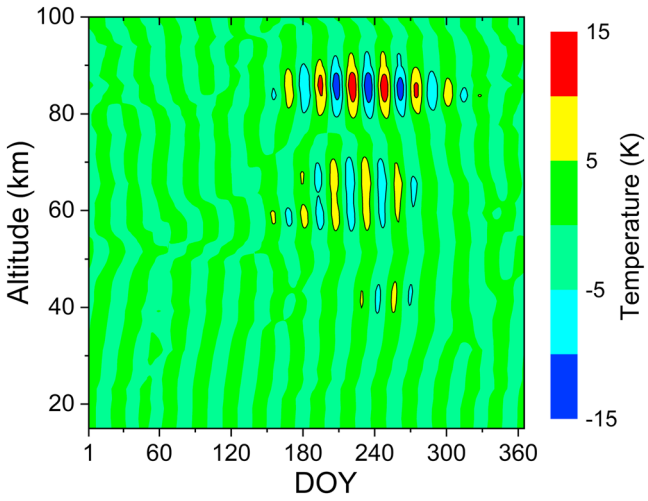

Figure 9. Band-pass filtered (24–30 days) Solar Occultation For Ice Experiment (SOFIE) temperatures perturbation between 270°E and 300°E identifying the evolution of the vertical extent of this event which exhibited a peak at ~85 km and an onset around DOY 150. The Solar Occultation For Ice Experiment (SOFIE) temperature measurements for 2014 covered the latitude range 48°S to 72°S. DOY = day of year.

the period when the 28-day oscillation was observed. In particular, this event was only evident between 240°E and 360°E longitude and was centered at ~285°E, with four cycles and peak amplitudes >10 K at MLT altitudes. The longitudinal coverage of this event was observed to increase with time, spanning ~180° in longitude at the peak of the event by late August, near the end of the austral winter. The longitudinal extent then reduced as the amplitude of the wave decreased in the early spring time. This result is fully consistent with our ground-based observations of a large MLT oscillation over Rothera station (longitude 292°E) but no evidence of a similar response over Davis station (longitude 78°E).

To further compare satellite temperature measurements with the ground-based results of this wave event, Figure 11 combines the band-pass filtered temperature results from SP station, Rothera station, and SOFIE at 85 km, between 270°E and 300°E longitude where the wave was strongest, as determined in Figure 10. The addition of the SOFIE data provides a complete picture of this extraordinary event. All three data sets reveal strong in-phase oscillations that started around DOY 150 (late May early June) during the austral winter. Up to six full oscillations were observed by SOFIE, establishing the lifetime of this event (~180 days). The amplitudes of the oscillation grew uniformly together, reaching a peak of ~15 K at around DOY 220 (8 August

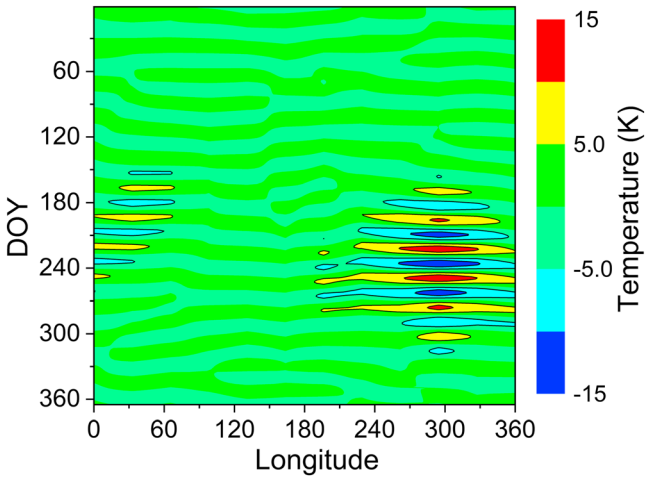

Figure 10. Same band-pass filtered SOFIE temperature perturbations as a function of longitude at 85-km altitude, identifying the localized signature of this prominent wintertime event at Mesosphere and Lower Thermosphere (MLT) altitudes. DOY = day of year.

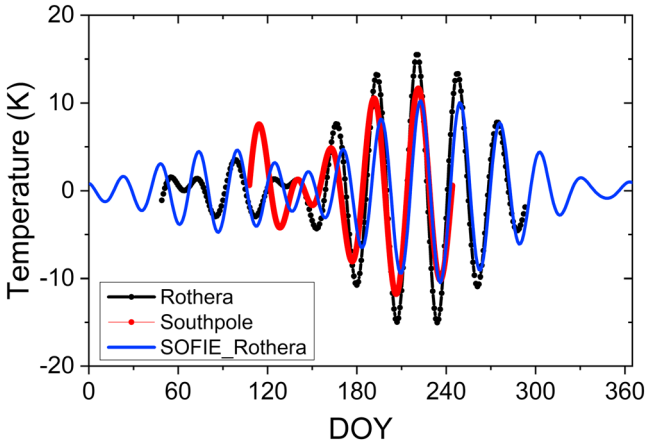

Figure 11. Comparison of ground-based and satellite temperature measurements of the 28-day oscillation revealing the full life cycle of this event. The SOFIE temperature data were plotted at 85 km, between 270°E and 300°E longitude where the amplitudes were largest at Mesosphere and Lower Thermosphere altitudes. SOFIE = Solar Occultation For Ice Experiment; DOY = day of year.

2014) and then decayed, producing a coherent symmetrical wave packet. Among these three data sets, Rothera station exhibited the largest wave perturbations.

Figures 9 and 10 have revealed the time evolution of the vertical and zonal structure of this oscillation in the Southern Hemisphere. Now we explore the vertical and zonal structure for 1 day in the cycle. Figure 12 plots the vertical structure versus longitudes for DOY 223 (close to maximum amplitude) using the SOFIE temperature data. A well-defined zonal wave #1 pattern is evident below 80 km, exhibiting larger amplitudes in the 0–60°E longitude sector. However, above 80 km, the data were dominated by a single strong maximum centered around 300°E, with no evidence of a corresponding minimum. Examination of other dates during the 2014 winter confirmed this finding of a single maximum (or minimum) at MLT altitudes. This further explains why the ground-based OH observations of this oscillation over Antarctica were stronger at Rothera station (292°E; and SP) but apparently absent at Davis station (78°E). However, it is important to note that at altitudes below ~80 km, SOFIE data did detect a strong 28-day response over Davis station (which was larger than the opposite peak over western Antarctica). Furthermore, the vertical structure of this PW indicates a vertical wavelength of ~35–40 km with clear horizontal zonal wave #1 structure.

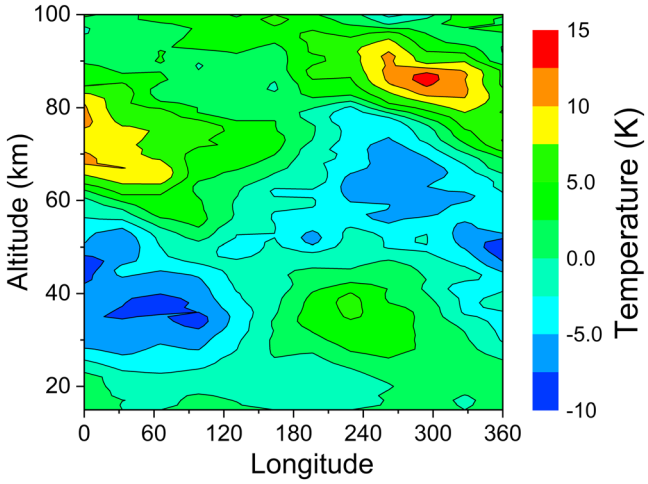

Figure 12. Solar Occultation For Ice Experiment temperature perturbation on DOY 223(11 August) plotting vertical structure as a function of longitude, revealing clear zonal wave #1 perturbation below 80 km. Above this height, the event is strongly localized in longitude (between ~240°E and 360°E) as also evident in Figure 10.

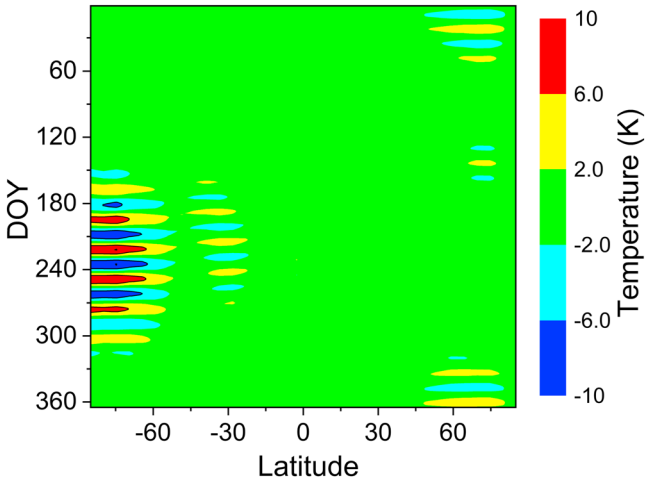

Figure 13. North-south cross section showing band-pass filtered Microwave Limb Sounder temperature data at 0.00464 hPa (at ~82 km) between 270°E and 300°E longitude, establishing the southern high-latitude wintertime signature of this event. Note also the weak low-latitude response at ~30ºS. DOY = day of year.

The 2014 MLS temperature measurements are now used to investigate the meridional extent (north-south) of this oscillation at MLT altitudes. The MLS data were binned into 5° latitude by 30° longitude sectors, and the same 24–30 day band-pass filter was applied to each bin for all pressure levels. Figure 13 presents the filtered results at 0.00464 hPa (at ~82 km) centered on 285°E longitude (between 270°E and 300°E), where the maximum response was measured by SOFIE (Figure 10). The MLS latitude versus DOY plot shows a strong localized oscillation during the wintertime in the southern polar region initiating ~DOY 150, near end of May, and exhibiting four strong cycles with peak amplitudes of ~10 K. The oscillation extended equatorward to ~60°S only. Close inspection of Figure 13 showed that at ~30°S, there was a secondary set of weaker wave extending from DOY 180 to ~DOY 270 with amplitudes of ~3 K at 82 km.

Examination of the SOFIE and MLS data at lower altitudes (below 80 km) has revealed a different zonal and latitudinal structure than that determined in the mesopause region. For example, Figure 14 plots the longitudinal structure versus DOY derived from the SOFIE band-pass filtered results at 30-km altitude in the Southern Hemisphere (using the same 30° longitudinally binned data). This altitude was chosen to coincide with the well-defined wave #1 structure in the stratosphere as seen in Figure 12. Comparison

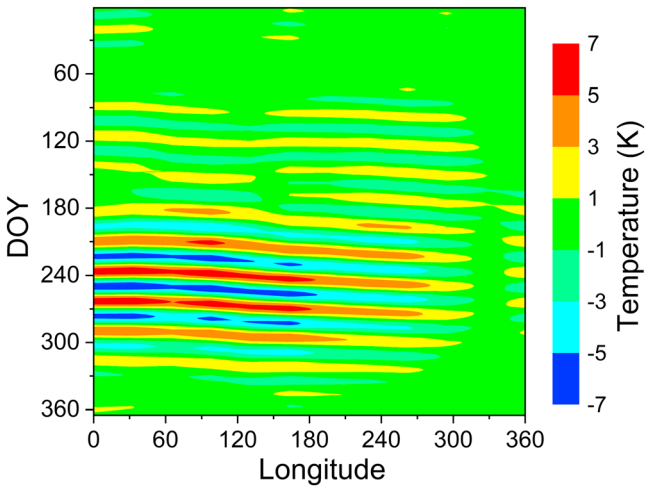

Figure 14. Band-pass filtered Solar Occultation For Ice Experiment temperature perturbations at 30 km showing the large longitudinal extent of this oscillation at stratospheric height. DOY = day of year.

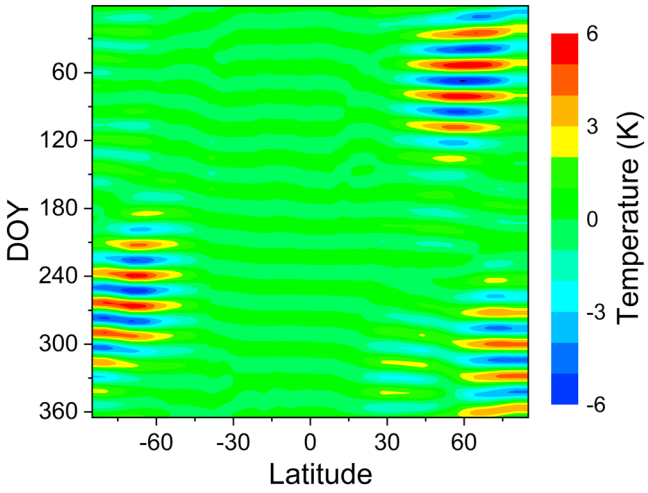

Figure 15. Same format as Figure 13 plotting Microwave Limb Sounder temperature perturbations at 10 hPa, firmly establishing the existence of this wave in both winter hemispheres in the stratosphere. DOY = day of year.

with the MLT results of Figure 10, the stratospheric zonal structure was surprisingly different. In particular, at stratospheric altitudes, the oscillation extended over all longitudes in contrast to the localized response observed in the MLT region. Furthermore, in the stratosphere, the oscillation was strongest between longitudes 0°E and 180°E and weakest between 300°E and 360°E where the amplitude was almost halved.

Based on the unexpected SOFIE results of the broad longitudinal extent of the event at 30 km (Figure 14), we have reexamined the MLS band-pass filtered temperature results at a similar altitude of 10 hPa (~30 km) to investigate the meridional extent of this oscillation. Figure 15 reproduces the format of Figure 13 but plotting the latitude versus DOY results at 10 hPa. Unlike the weak oscillation at 85 km in the Northern Hemisphere MLT region, which is due to the peak in the Northern Hemisphere winter located at much lower altitude (see Figure 17), the stratospheric signature yields a strong wintertime response equal to that of the Southern Hemisphere winter response, strongly suggesting that the 28-day oscillation is a high-latitude wintertime global phenomenon in both hemispheres. A secondary weak oscillation (amplitude 2–3 K) was also evident in the Northern Hemisphere in November and December at this lower stratospheric altitude but not for the Southern Hemisphere wintertime.

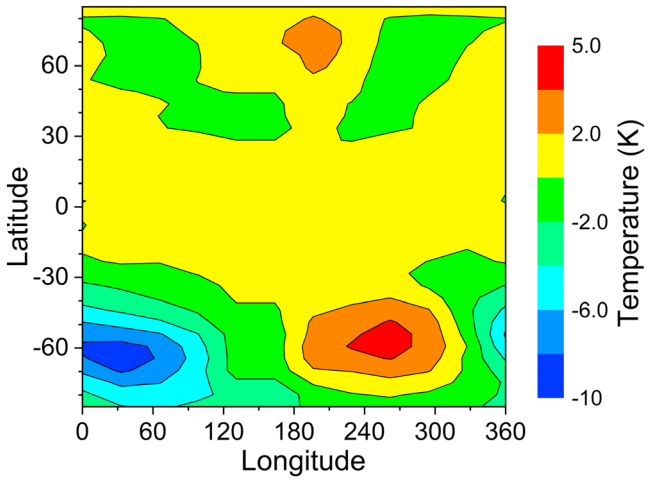

Figure 16. Example of the latitudinal and longitudinal structure of the 28-day oscillation at 10 hPa (~30 km) using Microwave Limb Sounder temperature on day of year 247 (4 September).

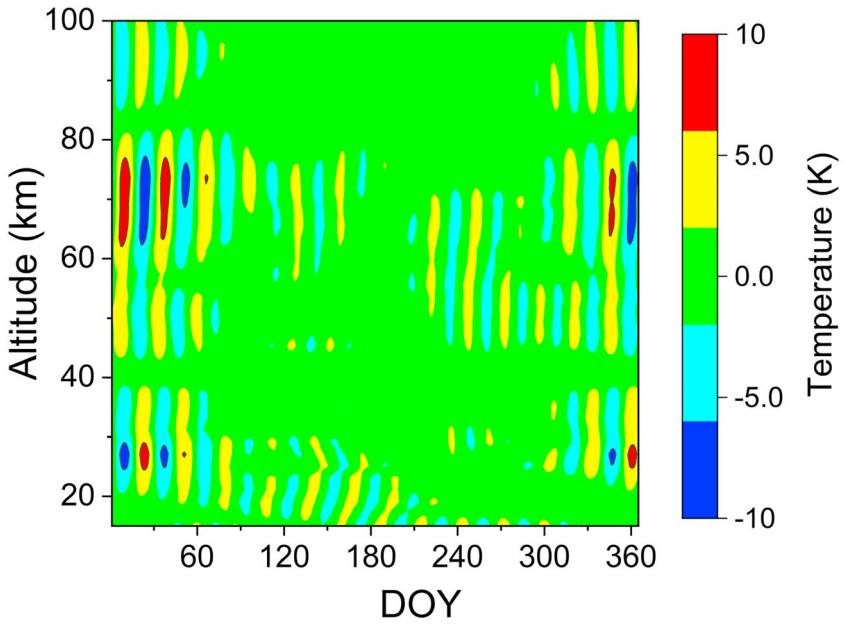

Figure 17. Same as Figure 9 but showing the Northern Hemisphere Solar Occultation For Ice Experiment band-pass filtered temperature perturbations for comparison. The peak altitude was at ~70 km, lower than the Southern Hemisphere peak. DOY = day of year.

Figure 16 plots stratospheric signature of the oscillation at 10 hPa using the MLS data on DOY 247. The plot clearly shows a zonal wave #1 structure consistent with our findings in Figure 12 below 80 km. Figure 16 further shows that this event extended from the Southern Hemisphere winter polar region to midlatitudes, peaking around 60°S. As now expected, no similar oscillation was detected in the summer time Northern Hemisphere, confirming the wintertime nature of this event. It is also important to note that the amplitude of this oscillation is larger (~10 K) at ~30°E, as compared with a 5 K peak amplitude at ~250°E. This asymmetry in amplitudes is evident all the way up to 80 km as also shown in Figure 12.

In the above analysis, we note that there are also indications of this oscillation in the Northern Hemisphere at high latitudes during the winter months but with much reduced amplitudes at MLT altitudes (<50%, Figure 13 at 82 km). Figure 17 compares the vertical structure of this oscillation in the Northern Hemisphere to that in the Southern Hemisphere (Figure 9, between 270°E and 300°E) using SOFIE temperature data. Both figures confirm that the 28-day oscillation occurred in the high-latitude wintertime in the Northern and Southern Hemispheres. However, Figure 17 shows this oscillation peaked at a lower altitude (~70 km) in the Northern Hemisphere as compared to that in the Southern Hemisphere (between 80 and 90 km). This explains why at 82 km (Figure 13) only very weak wave amplitudes were detected. In the Northern Hemisphere, the amplitudes of the 28-day oscillation (maximum ~9 K) were very similar to those observed in the Southern Hemisphere data (Figure 9). The temporal evolution and duration of this event were also similar, further establishing its existence in both the Northern and Southern Hemispheres during wintertime.

4. Discussion

Together, our analysis and results have firmly established this unusual 28-day oscillation as a wintertime, global-scale, vertically extensive and long lasting event exhibiting a wave #1 signature below 80 km.

One possible origin of this 28-day oscillation is the normal mode Rossby wave. Theoretically, one of the westward propagating modes of Rossby waves is the wave #1, meridional index (l-s) = 4 asymmetric mode, which has a period of 28.08 days in the presence of zonal winds (Kasahara, 1980; Madden, 2007) and a period of ~17 days with no zonal winds (Kasahara, 1980). This mode is sometimes referred as the 25-day free Rossby wave (Sassi et al., 2012). Rossby waves are westward propagating waves, and the (1,4) 28-day mode

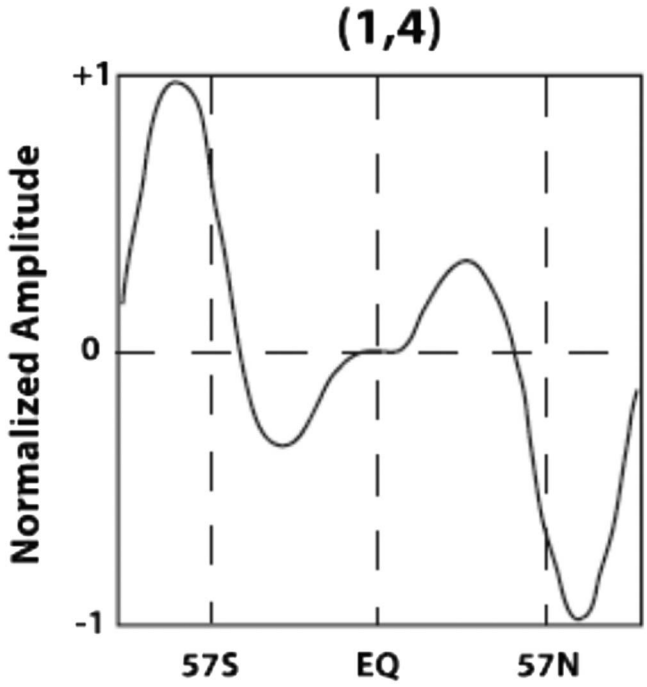

Figure 18. Figure 1 of Sassi et al. (2012) showing the theoretical latitudinal structure of the Rossby wave (1,4) mode in geopotential height (same latitudinal structure as temperature). Note the large amplitudes at high latitudes and the secondary amplitudes at lower latitudes.

has a very low phase speed (<10 m/s at high latitudes) which severely limits its propagation into the MLT during the summer. Sassi et al. (2012) also studied this Rossby (1,4) mode and found that propagation to higher altitudes was expected to be transient due to the background wind filtering. Figure 18 replots part of Figure 1 of Sassi et al. (2012) showing the latitudinal structure of this (1,4) mode for geopotential height (note that the latitudinal structure for temperature is the same). The figure is characterized by two large amplitude peaks at high latitudes of opposite signs and another two weaker peaks in the midlatitude regions. The satellite temperature results (Figures 13 and 15) have established that the 28-day oscillation peaked at high latitudes (~60°S and ~60°N) in both hemispheres and extended from the lower stratosphere to MLT altitudes with a zonal wave number1 structure below 80 km (Figures 12 and 16). Figures 13 and 15 also indicate possible secondary peaks at lower latitudes (~30°S and ~30°N). These signatures of this 28-day oscillation are consistent with the theoretic prediction of the Rossby (1,4) mode.

However, our analysis also revealed differences between the observed 28-day oscillation and the theoretical properties of the Rossby wave (1,4) mode, especially above 80 km. For example, Figures 10 and 12 showed the waves in the Southern Hemisphere exhibited stationary rather than propagating wave signatures which were only detected "locally." Furthermore, for a perfect zonal wave #1 wave, there should be no detectable signal at SP, contrary to the large observed oscillation reported herein. The causes of these discrepancies are possibly related to the ever changing background wind in the real atmosphere, filtering out the wave at one location (e.g., as for Davis station) and altering its apparent (observed) zonal phase speed. Nonetheless, the observed zonal and meridional signatures of this 28-day oscillation appear to be very similar to those of a westward propagating Rossby wave (1,4) mode.

Before we can draw this conclusion, we need to also address the possibility that this 28-day oscillation was driven directly by solar forcing. In addition to the well-known ~11-year solar cycle, the Sun rotates with a period of ~27 days and the associated solar radiation variation is known to modulate the Earth's atmospheric thermal structure and chemistry, with a similar periodicity, especially in the middle and upper atmosphere (e.g., Bossay et al., 2015; Ruzmaikin et al., 2007; Shapiro et al., 2012). In particular, Beig et al. (2008) reviewed solar driven 27-day oscillations in temperature and determined them to be

small (<4 K) in the mesosphere for all latitudes. More recently, Thomas et al. (2015) studied the effects of the 27-day solar variations on temperature during the polar summer season also using SOFIE temperature measurements. Their results showed that the maximum temperature response to solar variations was ~1 K. Both of these studies indicate solar-driven temperature changes are much smaller compared to the amplitude of the 28-day oscillation (~15 K) that was independently measured during the wintertime over Antarctica. Furthermore, several of the characteristics of this oscillation cannot be explained by the effects of solar radiance changes. For example, (a) the observed oscillation exhibited a clear zonal wave #1 structure below 80 km with well-defined vertical wave structure, (b) the event was restricted to wintertime at high latitudes, and (c) the wave spectrum (Figure 6) was broad and observed to change with time. Thus, while it is possible that a small fraction of the observed 28-day oscillation may have been due to direct solar forcing, the majority of this unusually strong 28-day oscillation was more likely the signature of a large amplitude (1,4) mode of Rossby wave. This said, it is also possible that the normal mode was triggered by the solar 27-day variation.

5. Summary

The PW activity in the MLT region over Antarctica during the 2014 winter season was dominated by a prominent (approximately six full cycles) large-amplitude 28-day oscillation. We have utilized ground-based OH temperature measurements from SP and Rothera stations together with satellite temperature profiles from MLS and SOFIE to investigate the temporal characteristics and spatial structure of this unusual event. The main findings are as follows:

1. Unusually strong (~15 K amplitude), persistent (~6 months) 28-day oscillation detected in 2014 winter/early spring temperature data over Antarctica.
2. Coherent vertical PW structure from stratosphere to MLT region showing amplitude growth with altitude (with peak in upper mesosphere) in both hemispheres during wintertime.
3. Below 80 km, the 28-day oscillation exhibited a clear zonal wave # 1 structure. Above 80 km, only a single peak was observed (probably due to wind filtering).
4. The 28-day oscillation was found to peak at high latitudes in both hemispheres and a secondary weak peak is evident at lower latitudes.
5. The observed zonal and meridional characteristics and the period of the 28-day oscillation are consistent with the theoretical signatures of the Rossby wave (1,4) mode.

To our best knowledge, this is the first time that such a strong long period (28 days), persistent PW has been observed in mesospheric temperature over Antarctica.

Appendix A: Statistical Significance of the Observed 28-Day Wave

The SP AMTM raw measurements used in this paper are irregularly spaced and contain data gaps, making the Lomb-Scargle analysis described in Press et al. (1992) an appropriate method for generating periodograms. However, the associated significance testing assumes a null hypothesis spectrum that is independent of period (i.e., it is white). Noting that "persistence" typical of atmospheric observations (e.g. Wilks, 2011) implies that successive data points are not independent, an alternate null hypothesis spectrum is needed. These concepts are captured in significance testing methods described in Wilks (2011) and used by Sassi et al. (2012) for their PW analysis. Here we describe their application in the context of the observed 2014 SP 28-day wave.

The persistence noted above can be described using an autoregressive model of order 1 (AR1) such that

$$T_{i+1}-\mu = \rho(T_i-\mu) + \varepsilon_{i+1}, \tag{A1}$$

where T_i and T_{i+1} are successive temperature measurements in our time series, μ is the time series mean, ρ is the lag-1 autocorrelation parameter, and $\varepsilon_{i+1}$is a random (uncorrelated) quantity with zero mean and a variance σ_ε^2 which is independent of frequency (Wilks, 2011). The AR1 process has a theoretical spectral density function related to the above parameters by

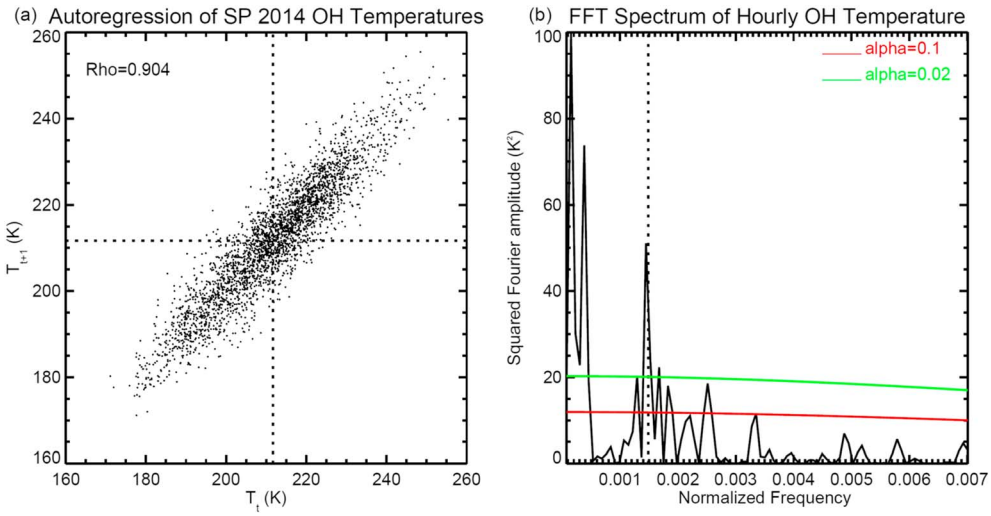

Figure A1. (a) South Pole Advanced Mesospheric Temperature Mapper hourly average temperatures for 2014 plotted against their one-point lagged counterparts. Dashed lines indicate the mean. (b) Frequency spectrum of squared Fourier amplitudes expressed in terms of normalized frequency. The vertical line indicates the frequency of a 28-day oscillation. The colored lines show 90% (red) and 98% (green) significance levels for assumptions discussed in the text.

$$S(f) = \frac{4\sigma_\varepsilon^2 / n}{1 + \rho^2 - 2\rho\cos(2\pi f)}, 0 \le f \le 1/2 \tag{A2}$$

where n is the number of points in the time series and f is a normalized frequency such that the Nyquist frequency falls at $f = 1/2$ (Wilks, 2011). The quantity σ_ε^2 can be obtained from the variance of the time series σ_T^2 using $\sigma_\varepsilon^2 = (1-\rho^2)\,\sigma_T^2$ (Wilks, 2011).

The kth Fourier component of the observed spectrum C_k^2 can be deemed significant at the $(1-\alpha)$ level if

$$\frac{\upsilon C_k^2}{S(f)} > \chi_\upsilon^2(1-\alpha), \text{or } C_k^2 > \chi_\upsilon^2(1-\alpha)\frac{S(f)}{\upsilon}, \tag{A3}$$

where $\chi_\upsilon^2(1-\alpha)$ is the value of the chi-square distribution for a significance level of $(1-\alpha)$ and number of degrees of freedom υ.

To extract the Fourier components needed for this analysis, the SP AMTM temperatures during 2014 were resampled into hourly bins. The periodogram shown in Figure 4 oversamples in frequency by a factor of 4. Thus, in order to reproduce the Lomb-Scargle analysis results using an FFT, the time series needs to be extended ("zero padded") by a factor of 4 to decrease the output frequency interval. Excellent agreement between the form of the two periodograms is obtained when this is done (not shown), demonstrating the equivalence of the two methods of analysis. However, it is noted that the zero padding does not change the information content of the periodogram.

Figure A1a shows the utility of an AR1 model for these data. Here, hourly averages of the SP AMTM temperatures during 2014 are plotted against the hourly temperature that follows and a strong correlation is apparent. The parameter ρ is calculated (Wilks, 2011) and has a value of 0.904. The time series variance σ_T^2 yields a value of σ_ε^2 of 35.295 using the equation given above.

To obtain the value of C_k^2, an FFT is applied (with a transform direction that does not scale by the number of points) to the zero padded time series and the positive and negative frequency components are summed (to give a single-sided spectrum). The squared amplitude of each Fourier component is obtained by multiply the complex spectral amplitudes by their complex conjugate and dividing by the square of the number of points n. The low-frequency part of the resulting spectrum is shown in Figure A1b, with a normalized frequency scale as defined above. The number of points n used here and in the theoretical AR1 spectrum is equal to the number of good data points in the time series. Thus, the influence of data gaps and zero padding is excluded. The peak corresponding to a 28-day period (indicated by a vertical line) implies an amplitude of $\sqrt{51} \approx 7$K which is consistent with oscillations in the observed time series.

The statistical significance criterion given in equation (A3) above can be assessed by scaling the theoretical spectrum $S(f)$ (for which all the parameters are now known) with χ^2_υ and υ. The number of degrees of freedom used here is $\upsilon = 2$ because the squared amplitude is generated from two independent parameters (Wilks, 2011). To test for the presence of a wave of period known to be 28 days at the 90% level in Figure A1, the squared amplitude coefficients need to exceed the line associated with $\alpha = 0.1$. (It is noted that no smoothing has been applied to this spectrum.) The peak at 28 days is thus significant at that level. However, without a priori knowledge of the period, it is necessary test whether the largest peak in the vicinity of a 28-day period is significant. Here we choose a band of five frequencies around our frequency of interest and note that a smaller level of $\alpha = {}^{0.1}/_{5} = 0.02$ is required (Wilks, 2011). In this case, the peak value and two nearby peaks satisfy the significance condition. As such we assert that the 28-day oscillation is present to at least a 90% confidence level.

Acknowledgments
The AMTM data from SP are available online (http://digitalcommons.usu.edu/ail/. Password to access the database can be provided upon request to the authors). The Rothera temperature data are available online (http://psddb.nerc-bas.ac.uk/data/access/coverage.php?menu=4&bc=1&source=1&class=46&year=2014). Davis data are available through a website (http://data.aad.gov.au/metadata/records/Davis_OH_airglow). The SOFIE data are available as standard data products online (http://sofie.gats-inc.com/sofie/index.php). MLS data are available online (https://disc.gsfc.nasa.gov/datasets?page=1&keywords=ML2T_004). This investigation was supported by NSF OPP ANGWIN program under contract 1443730 and NASA AIM mission under contract NAS5-03132 (subcontract from Hampton University to Utah State University 05-17). The South Pole data collection was supported by NSF 1143587. We would like to thank the wintering engineer support teams at SP and Rothera and the NERC Polar Data Centre staff. Davis OH temperature data collection was supported under Australian Antarctic Science project 4157. We would also like to thank Dr. Jeff Forbes for his very helpful PW discussion. We would like to acknowledge the MLS team for their temperature data used in this study. Finally, we thank the reviewers for their very helpful comments.

References

Azeem, S. M. I., & Sivjee, G. G. (2009). Multiyear observations of tidal oscillations in OH M (3,1) rotational temperatures at South Pole, Antarctica. *Journal of Geophysical Research*, *114*, A06312. https://doi.org/10.1029/2008JA013976

Azeem, S. M. I., Sivjee, G. G., Won, Y.-I., & Mutiso, C. (2007). Solar cycle signature and secular long-term trend in OH airglow temperature observations at South Pole, Antarctica. *Journal of Geophysical Research*, *112*, A01305. https://doi.org/10.1029/2005JA011475

Baker, D. J., & Stair, A. T. Jr. (1988). Rocket measurements of the altitude distributions of the hydroxyl airglow. *Physica Scripta*, *37*, 611.

Beig, G., Scheer, J., Mlynczak, M. G., & Keckhut, P. (2008). Overview of the temperature response in the mesosphere and lower thermosphere to solar activity. *Reviews of Geophysics*, *46*, RG3002. https://doi.org/10.1029/2007RG00236

Bossay, S., Bekki, S., Marchand, M., Poulain, V., & Toumi, R. (2015). Sensitivity of tropical stratospheric ozone to rotational UV variations estimated from UARS and Aura MLS observations during the declining phases of solar cycles 22 and 23. *Journal of Atmospheric and Solar - Terrestrial Physics*, *130-131*, 96–111. https://doi.org/10.1016/j.jastp.2015.05.014

Cai, X., Yuan, T., Zhao, Y., Pautet, P.-D., Taylor, M. J., & Pendleton, W. R. Jr. (2014). A coordinated investigation of the gravity wave breaking and the associated dynamical instability by a Na lidar and an advanced mesosphere temperature mapper over Logan, UT (41.7° N, 111.8° W). *Journal of Geophysical Research: Space Physics*, *119*, 6852–6864. https://doi.org/10.1002/2014JA020131

Chu, X., Pan, W., Papen, G. C., Gardner, C. S., & Gelbwachs, J. A. (2002). Fe Boltzmann temperature lidar: Design, error analysis, and initial results at the North and South Poles. *Applied Optics*, *41*(21), 4400–4410. https://doi.org/10.1364/AO.41.004400

Day, K. A., & Mitchell, N. J. (2010). The 5-day wave in the Arctic and Antarctic mesosphere and lower thermosphere. *Journal of Geophysical Research*, *115*, D01109. https://doi.org/10.1029/2009JD012545

Demissie, T. D., Kleinknecht, N. H., Hibbins, R. E., Espy, P. J., & Straub, C. (2013). Quasi-16 day period oscillations observed in middle atmospheric ozone and temperature in Antarctica. *Annales de Geophysique*, *31*(7), 1279–1284. https://doi.org/10.5194/angeo-31-1279-2013

Dowdy, A. J., Vincent, R. A., Murphy, D. J., Tsutsumi, M., Riggin, D. M., & Jarvis, M. J. (2004). The large-scale dynamics of the mesosphere–lower thermosphere during the Southern Hemisphere stratospheric warming of 2002. *Geophysical Research Letters*, *31*, L14102. https://doi.org/10.1029/2004GL020282

Espy, P. J., Hibbins, R. E., Jones, G. O. L., Riggin, D. M., & Fritts, D. C. (2003). Rapid, large-scale temperature changes in the polar mesosphere and their relationship to meridional flows. *Geophysical Research Letters*, *30*(5), 1240. https://doi.org/10.1029/2002GL016452

Espy, P. J., Hibbins, R. E., Riggin, D. M., & Fritts, D. C. (2005). Mesospheric planetary waves over Antarctica during 2002. *Geophysical Research Letters*, *32*, L21804. https://doi.org/10.1029/2005GL023886

Espy, P. J., & Stegman, J. (2002). Trends and variability of mesospheric temperature at high latitudes. *Physics and Chemistry of the Earth*, *27*(6-8), 543–553. https://doi.org/10.1016/S1474-7065(02)00036-0

Espy, P. J., Stegman, J., Forkman, P., & Murtagh, D. (2007). Seasonal variation in the correlation of airglow temperature and emission rate. *Geophysical Research Letters*, *34*, L17802. https://doi.org/10.1029/2007GL031034

Forbes, J. M., Portnyagin, Y. I., Makarov, N. A., Palo, S. E., Merzlyakov, E. G., & Zhang, X. (1999). Dynamics of the lower thermosphere over South Pole from meteor radar wind measurements. *Earth, Planets and Space*, *51*(7-8), 611–620. https://doi.org/10.1186/BF03353219

Fraser, G. J., Hernandez, G., & Smith, R. W. (1993). Eastward-moving 2-4 day waves in the winter Antarctic mesosphere. *Geophysical Research Letters*, *20*(15), 1547–1550. https://doi.org/10.1029/93GL01707

French, W. J. R., Burns, G. B., & Espy, P. J. (2005). Anomalous winter hydroxyl temperatures at 69°S during 2002 in a multiyear context. *Geophysical Research Letters*, *32*, L12818. https://doi.org/10.1029/2004GL022287

French, W. J. R., & Klekociuk, A. R. (2011). Long-term trends in Antarctic winter hydroxyl temperatures. *Journal of Geophysical Research*, *116*, D00P09. https://doi.org/10.1029/2011JD015731

Gordley, L. L., Hervig, M. E., Fish, C., Russell, J. M. III, Bailey, S., Cook, J., et al. (2009). The solar occultation for ice experiment. *Journal of Atmospheric and Solar - Terrestrial Physics*, *71*(3-4), 300–315. https://doi.org/10.1016/j.jastp.2008.07.012

Hernandez, G. (2003). Climatology of the upper mesosphere temperature above South Pole (90°S): Mesospheric cooling during 2002. *Geophysical Research Letters*, *30*(10), 1535. https://doi.org/10.1029/2003GL016887

Hernandez, G., Smith, R. W., & Conner, J. F. (1992). Neutral wind and temperature in the upper mesosphere above south pole, Antarctica. *Geophysical Research Letters*, *19*(1), 53–56. https://doi.org/10.1029/91GL02957

Hernandez, G. R., Smith, W., Kelley, J. M., Fraser, G. J., & Clark, K. C. (1997). Mesospheric standing waves near South Pole. *Geophysical Research Letters*, *24*(16), 1987–1990. https://doi.org/10.1029/97GL01999

Hervig, M. E., Gerding, M., Stevens, M. H., Stockwell, R., Bailey, S. M., Russell, J. M., & Stober, G. (2016). Mid-latitude mesospheric clouds and their environment from SOFIE observations. *Journal of Atmospheric and Solar - Terrestrial Physics*, *149*, 1–14. https://doi.org/10.1016/j.jastp.2016.09.004

Hervig, M. E., & Gordley, L. L. (2010). The temperature, shape, and phase of mesospheric ice from SOFIE observations. *Journal of Geophysical Research*, *115*, D15208. https://doi.org/10.1029/2010JD013918

Kasahara, A. (1980). Effect of zonal flows on the free oscillations of a barotropic atmosphere. *Journal of the Atmospheric Sciences*, *37*(5), 917–929. https://doi.org/10.1175/1520-0469(1980)037<0917:EOZFOT>2.0.CO;2

Lawrence, B. N., Fraser, G. J., Vincent, R. A., & Phillips, A. (1995). The 4-day wave in the Antarctic mesosphere. *Journal of Geophysical Research*, *100*(D9), 18,899–18,908.

Lieberman, R. S., & Riggin, D. (1997). High resolution Doppler imager observations of Kelvin waves in the equatorial mesosphere and lower thermosphere. *Journal of Geophysical Research*, *102*(D22), 26,117–26,130.

Luo, Y., Manson, A. H., Meek, C. E., Igarashi, K., & Jacobi, C. (2001). Extra long period (20–40 day) oscillations in the mesospheric and lower thermospheric winds: Observations in Canada, Europe and Japan, and considerations of possible solar influences. *Journal of Atmospheric and Solar - Terrestrial Physics*, *63*(9), 835–852. https://doi.org/10.1016/S1364-6826(00)00206-6

Madden, R. A. (2007). Large-scale, free Rossby waves in the atmosphere—An update. *Tellus*, *59A*, 571–590.

Meriwether, J. W. Jr. (1975). High latitude airglow observations of correlated short-term fluctuations in the hydroxyl Meinel 8-3 band intensity and rotational temperature. *Planetary and Space Science*, *23*(8), 1211–1221. https://doi.org/10.1016/0032-0633(75)90170-1

Murphy, D. J., French, W. J. R., & Vincent, R. A. (2007). Long-period planetary waves in the mesosphere and lower thermosphere above Davis, Antarctica. *Journal of Atmospheric and Solar - Terrestrial Physics*, *69*(17-18), 2118–2138. https://doi.org/10.1016/j.jastp.2007.06.008

Palo, S. E., Portnyagin, Y. I., Forbes, J. M., Makarove, N. A., & Merzlyakov, E. G. (1998). Transient eastward propagating long-period waves observed over the South Pole. *Annales de Geophysique*, *16*, 1586–1500.

Pan, W., & Gardner, C. S. (2003). Seasonal variations of the atmospheric temperature structure at South Pole. *Journal of Geophysical Research*, *108*(D18), 4564. https://doi.org/10.1029/2002JD003217

Pautet, P.-D., Taylor, M. J., Pendleton, W. R. Jr., Zhao, Y., Yuan, T., Esplin, R., & McLain, D. (2014). Advanced mesospheric temperature mapper for high-latitude airglow studies. *Applied Optics*, *53*(26), 5934–5943. https://doi.org/10.1364/AO.53.005934

Pautet, P.-D., Taylor, M. J., Snively, J. B., & Solorio, C. (2018). Unexpected occurrence of mesospheric frontal gravity wave events over South Pole (90°S). *Journal of Geophysical Research: Atmospheres*, *123*, 160–173. https://doi.org/10.1002/2017JD027046

Pendleton, W. R. Jr., Taylor, M. J., & Gardner, L. C. (2000). Terdiurnal oscillations in OH Meinel rotational temperatures for fall conditions at northern midlatitude sites. *Geophysical Research Letters*, *27*(12), 1799–1802. https://doi.org/10.1029/2000GL003744

Press, W. H., Teukolsky, S. A., Vetterling, W. T., & Flannery, B. P. (1992). *Numerical recipes in C: The art of scientific computing*, (Second ed.). Cambridge: Cambridge University Press.

Riggin, D., Fritts, D. C., Tsuda, T., Nakamura, T., & Vincent, R. A. (1995). Radar observations of a 3-day Kelvin wave in the equatorial mesosphere. *Journal of Geophysical Research*, *102*, 26,141–26,157.

Russell, J. M. III, Bailey, S. M., Horanyi, M., Gordley, L. L., Rusch, D. W., Hervig, M. E., et al. (2009). Aeronomy of ice in the mesosphere (AIM): Overview and early science results. *Journal of Atmospheric and Solar - Terrestrial Physics*, *71*(3-4), 289–299. https://doi.org/10.1016/j.jastp.2008.08.011

Ruzmaikin, A., Santee, M. L., Schwartz, M. J., Froidevaux, L., & Pickett, H. (2007). The 27-day variations in stratospheric ozone and temperature: New MLS data. *Geophysical Research Letters*, *34*, L02819. https://doi.org/10.1029/2006GL028419

Sassi, F., Garcia, R. R., & Hoppel, K. W. (2012). Large-scale Rossby normal modes during some recent Northern Hemisphere winters. *Journal of the Atmospheric Sciences*, *69*(3), 820–839. https://doi.org/10.1175/JAS-D-1-0103.1

Scargle, J. D. (1982). Studies in astronomical time series analysis. II. Statistical aspects of spectral analysis of unevenly spaced data. *The Astrophysical Journal*, *263*, 835–853. https://doi.org/10.1086/160554

Schoeberl, M. R. A., Douglass, R., Hilsenrath, E., Bhartia, P. K., Beer, R., Waters, J. W., et al. (2006). Overview of the EOS Aura mission. *IEEE Transactions on Geoscience and Remote Sensing*, *44*(5), 1066–1074. https://doi.org/10.1109/TGRS.2005.861950

Schwartz, J. J., Lambert, A., Manney, G. L., Read, W. G., Livesey, N. J., Froidevaux, L., et al. (2008). Validation of the Aura Microwave Limb Sounder temperature and geopotential height measurements. *Journal of Geophysical Research*, *113*, D15S11. https://doi.org/10.1029/2007JD008783

Shapiro, A. V., Rozanov, E., Shapiro, A. I., Wang, S., Egorova, T., Schmutz, W., & Peter, T. (2012). Signature of the 27-day solar rotation cycle in mesospheric OH and H_2O observed by the Aura Microwave Limb Sounder. *Atmospheric Chemistry and Physics*, *12*(7), 3181–3188. https://doi.org/10.5194/acp-12-3181-2012

Sivjee, G. G., & Walterscheid, R. L. (1994). Six-hour zonally symmetric tidal oscillations of the winter mesopause over the South Pole Station. *Planetary and Space Science*, *42*(6), 447–453. https://doi.org/10.1016/0032-0633(94)00085-9

Sivjee, G. G., & Walterscheid, R. L. (2002). Low-frequency intraseasonal variations of the wintertime very high latitude mesopause regions. *Journal of Geophysical Research*, *107*(A7), 1109. https://doi.org/10.1029/2001JA000164

Sivjee, G. G., Walterscheid, R. L., & McEwen, D. J. (1994). Planetary wave disturbances in the Arctic winter mesopause over Eureka (80°N). *Planetary and Space Science*, *42*(11), 973–986. https://doi.org/10.1016/0032-0633(94)90057-4

Stevens, M. H., Deaver, L. E., Hervig, M. E., Russell, J. M. III, Siskind, D. E., Sheese, P. E., et al. (2012). Validation of upper mesospheric and lower thermospheric temperatures measured by the solar occultation for ice experiment. *Journal of Geophysical Research*, *117*, D16304. https://doi.org/10.1029/2012JD017689

Stockwell, R. G., Riggin, D. M., French, W. J. R., Burns, G. B., & Murphy, D. J. (2007). Planetary waves and intraseasonal oscillations at Davis, Antarctica, from undersampled time series. *Journal of Geophysical Research*, *112*, D21107. https://doi.org/10.1029/2006JD008034

Taylor, M. J., Pendleton, W. R. Jr., Pautet, P.-D., Zhao, Y., Olsen, C., Surendra Babu, H. K., et al. (2007). Recent progress in mesospheric gravity wave studies using nightglow imaging system. *Revista Brasileira de Geofisica*, *25*, 49–58. https://doi.org/10.1590/S0102-261X2007000600007

Thomas, G. E., Thurairajah, B., Hervig, M. E., & von Savigny, C. (2015). Solar-induced 27-day variations of mesospheric temperature and water vapor from the AIM SOFIE experiment: Drivers of polar mesospheric cloud variability. *Journal of Atmospheric and Solar - Terrestrial Physics*, *134*, 56–68.

Torrence, C., & Compo, G. P. (1998). A practical guide to wavelet analysis. *Bulletin of the American Meteorological Society*, *79*(1), 61–78. https://doi.org/10.1175/1520-0477(1998)079%3C0061:APGTWA%3E2.0.CO;2

Tunbridge, V. M., & Mitchell, N. J. (2009). The two-day wave in the Antarctic and Arctic mesosphere and lower thermosphere. *Atmospheric Chemistry and Physics*, *9*(17), 6377–6388. https://doi.org/10.5194/acp-9-6377-2009

Walterscheid, R. L., Hecht, J. H., Gelinas, L. J., MacKinnon, A., Vincent, R. A., Reid, I. M., et al. (2015). Simultaneous observations of the phase-locked 2 day wave at Adelaide, Cerro Pachon, and Darwin. *Journal of Geophysical Research: Atmospheres*, *120*, 1808–1825. https://doi.org/10.1002/2014JD022016

Waters, J. W., Froidevaux, L., Harwood, R. S., Jarnot, R. F., Pickett, H. M., Read, W. G., et al. (2006). The Earth Observing System Microwave Limb Sounder (EOS MLS) on the Aura satellite. *IEEE Transactions on Geoscience and Remote Sensing*, *44*(5), 1075–1092. https://doi.org/10.1109/TGRS.2006.873771

Wilks, D. S. (2011). *Statistical Methods in the Atmospheric Sciences* (Vol. 100, 3rd ed., pp. 627–702). Oxford, UK: Academic Press.

Wu, D. L., Hays, P. B., & Skinner, W. R. (1994). Observations of the 5-day wave in the mesosphere and lower thermosphere. *Geophysical Research Letters*, *21*(24), 2733–2736. https://doi.org/10.1029/94GL02660

Zhao, Y., Taylor, M. J., Liu, H.-L., & Roble, R. G. (2007). Seasonal oscillations in mesospheric temperatures at low-latitudes. *Journal of Atmospheric and Solar - Terrestrial Physics*, *69*(17-18), 2367–2378. https://doi.org/10.1016/j.jastp.2007.07.010